Report

Current Biology

Plaid Detectors in Macaque V1 Revealed by Two-Photon Calcium Imaging

Highlights

- V1 responses to gratings and plaids are recorded with two-photon imaging in macaques
- Many non-orientation-tuned V1 neurons are strongly responsive to plaids
- Most orientation-tuned V1 neurons show cross-orientation inhibition
- Grating and plaid neurons together represent lines and line crossings precisely

Authors

Shu-Chen Guan, Sheng-Hui Zhang, Yu-Cheng Zhang, Shi-Ming Tang, Cong Yu

Correspondence

tangshm@pku.edu.cn (S.-M.T.), yucong@pku.edu.cn (C.Y.)

In Brief

Psychophysicists have long suspected that some early visual neural mechanisms might be responsible for plaid processing. In this two-photon calcium imaging study, Guan et al. confirm the existence of neurons in macaque V1 superficial layers that are not orientation tuned but are strongly responsive to plaids.

Guan et al., 2020, Current Biology *30*, 1–7
March 9, 2020
https://doi.org/10.1016/j.cub.2020.01.005

CellPress

Please cite this article in press as: Guan et al., Plaid Detectors in Macaque V1 Revealed by Two-Photon Calcium Imaging, Current Biology (2020), https://doi.org/10.1016/j.cub.2020.01.005

Current Biology
Report

Plaid Detectors in Macaque V1 Revealed by Two-Photon Calcium Imaging

Shu-Chen Guan,[1] Sheng-Hui Zhang,[1] Yu-Cheng Zhang,[2] Shi-Ming Tang,[1,3,4,*] and Cong Yu[1,2,4,5,*]
[1]PKU-Tsinghua Center for Life Sciences, Peking University, Beijing 100181, China
[2]School of Psychology and Cognitive Sciences, Peking University, Beijing 100181, China
[3]School of Life Sciences, Peking University, Beijing 100181, China
[4]IDG-McGovern Institute for Brain Research, Peking University, Beijing 100181, China
[5]Lead Contact
*Correspondence: tangshm@pku.edu.cn (S.-M.T.), yucong@pku.edu.cn (C.Y.)
https://doi.org/10.1016/j.cub.2020.01.005

SUMMARY

Neuronal responses to one-dimensional orientations are combined to represent two-dimensional composite patterns; this plays a key role in intermediate-level vision such as texture segmentation. However, where and how the visual cortex starts to represent composite patterns, such as a plaid consisting of two superimposing gratings of different orientations, remains neurophysiologically elusive. Psychophysical and modeling evidence has suggested the existence of early neural mechanisms specialized in plaid detection [1–6], but the responses of V1 neurons to an optimally orientated grating are actually suppressed by a superimposing grating of different orientation (i.e., cross-orientation inhibition) [7, 8]. Would some other V1 neurons be plaid detectors? Here, we used two-photon calcium imaging [9] to compare the responses of V1 superficial-layer neurons to gratings and plaids in awake macaques. We found that many non-orientation-tuned neurons responded weakly to gratings but strongly to plaids, often with plaid orientation selectivity and cross-angle selectivity. In comparison, most (~94%) orientation-tuned neurons showed more or less cross-orientation inhibition, regardless of the relative stimulus contrasts. Only a small portion (~8%) of them showed plaid facilitation at off-peak orientations. These results suggest separate subpopulations of plaid and grating responding neurons. Because most of these plaid neurons (~95%) were insensitive to motion direction, they were plaid pattern detectors, not plaid motion detectors.

RESULTS AND DISCUSSION

We recorded neuronal responses to Gabor gratings or plaid patterns in V1 superficial layers (II/III) in two awake macaque monkeys. Each plaid consisted of two superimposing Gabors with a cross-angle of 90° for monkey A, and of 30°, 60°, or 90° for monkey B (Figure 1A). Recordings were made 150 and 300 μm deep from the cortical surface. Initial screening with thresholding and size filtering of differential images (see STAR Methods) identified 2,709 cell bodies in monkey A and 2,094 in monkey B.

Each cell's responses (ΔF/F0) to Gabor orientations were then examined with a non-parametric Friedman test, which identified 1,300 (48.0%) orientation-tuned neurons in monkey A and 921 (44.0%) in monkey B. The remaining were classified as non-orientation-tuned neurons.

Plaid Detection in Non-orientation-tuned Neurons

Many non-orientation-tuned neurons responded strongly to plaid patterns (Figure 1B). Each "plaid" neuron was defined as having a peak plaid response significantly higher than the higher grating component response. There were 360 plaid neurons in monkey A (25.6% of non-orientation-tuned neurons, or 13.3% of all neurons) and 389 plaid neurons in monkey B (33.2% of non-orientation-tuned neurons, or 18.6% of all neurons).

Individually, plaid neurons A445 and A1238 from monkey A responded best to a 90° plaid orientation (the vector sum of two component grating orientations at 45° and 135°) (Figure 1B). The responses weakened at other plaid orientations, showing plaid orientation selectivity. Plaid neurons B60 and B1009 from monkey B responded best to 120° and 75° plaid orientations at cross-angles of 30° and 60°, respectively, showing plaid orientation selectivity and cross-angle selectivity. Plaid neurons B241 and B765 showed similar peak responses to plaids at three cross-angles, and at each cross-angle the responses weakened at non-optimal plaid orientations, showing plaid orientation selectivity but not cross-angle selectivity. At the least preferred plaid orientations, these neurons' plaid responses were comparable to grating component responses, which justified classifying plaid neurons by comparing the peak plaid response to the higher grating component response, rather than to the sum of grating component responses. 61.1% of plaid neurons in monkey A and 62.5% in monkey B were plaid orientation selective (Figure 1C). For monkey B, who was tested with three cross-angles, 32.3% plaid neurons were cross-angle selective (Figure 1D). Overall, only 4.3% of plaid neurons were sensitive to the plaid motion direction (Figure 1E).

To characterize plaid neurons' responses, we contrasted the peak plaid responses and higher grating component responses (Figure 1F). The median plaid response versus higher grating component response was 0.27 versus 0.09 in monkey A and 0.48 versus 0.17 in monkey B. We also calculated the plaid facilitation index (PFI) as

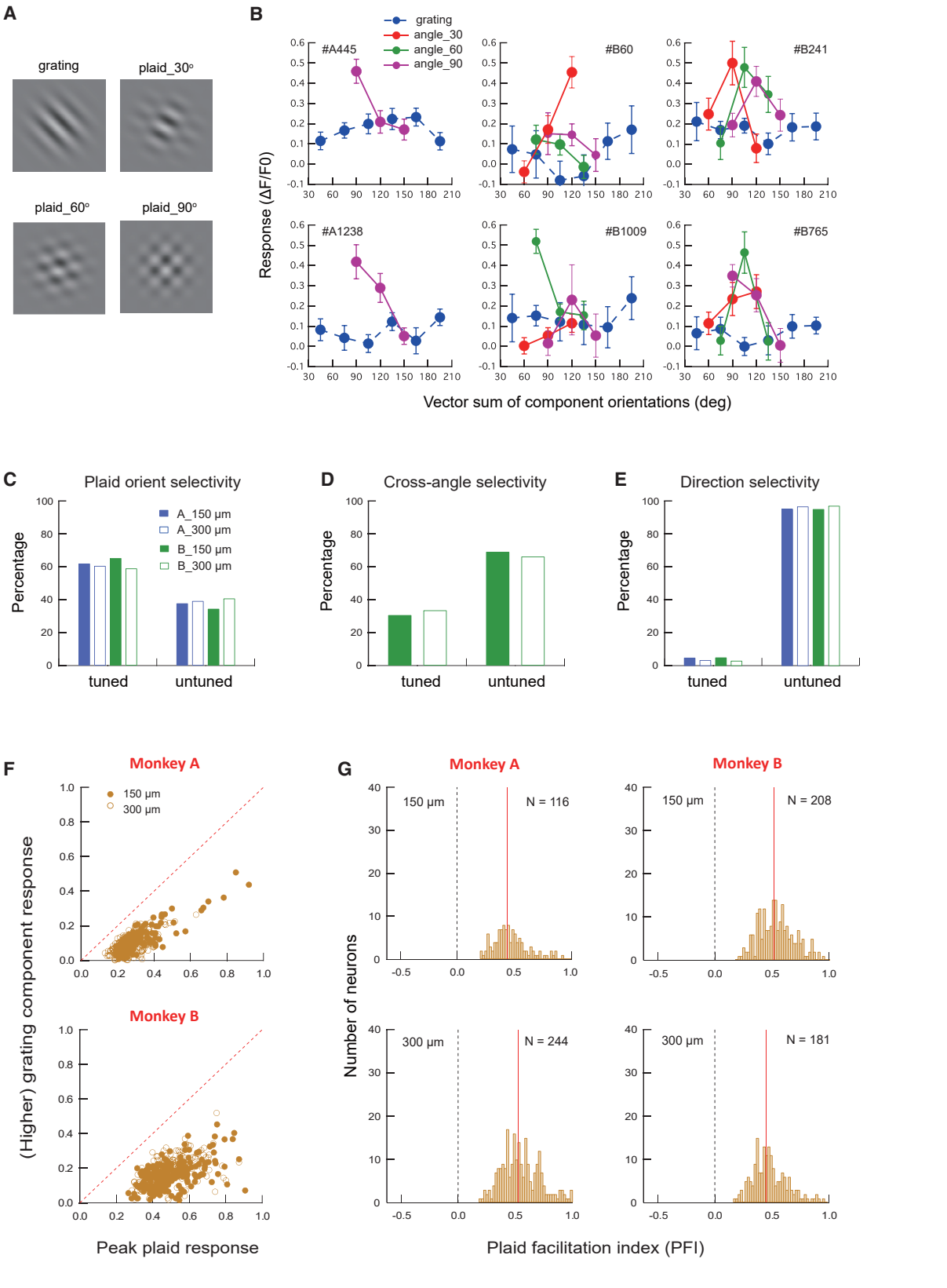

(legend on next page)

$$PFI = \frac{R_{max\_plaid} - R_{max\_comp}}{R_{max\_plaid} + R_{max\_comp}}, \quad \text{(Equation 1)}$$

where R_{max_plaid} was the neuron's peak plaid response and R_{max_comp} was the neuron's corresponding higher component response. PFI > 0 would indicate plaid facilitation. The median PFIs were 0.45 and 0.52 at 150 μm and 300 μm in monkey A, and 0.52 and 0.45 at 150 μm and 300 μm in monkey B, respectively (Figure 1E).

Cross-Orientation Inhibition in Orientation-Tuned Neurons

The peak responses of nearly all orientation-tuned neurons (or "grating neurons") were more or less suppressed by a superimposing grating at a non-optimal orientation. For example, for each exemplar neuron in Figure 2A, the peak response to an optimally oriented Gabor was suppressed by an orthogonal Gabor at the same contrast (0.32 for monkey A and 0.50 for monkey B), showing cross-orientation inhibition [7, 8, 10]. The median peak response was reduced by 54.9% in monkey A and 52.2% in monkey B, and there was little difference between the two recording depths. However, responses to grating orientations ±30° off the peak were much less affected by an orthogonal grating (Figure 2A). The peak responses of neurons B434 and B514 were also suppressed by gratings at 30° and 60° cross-angles (Figure 2A). Only 21.5% of grating neurons were cross-angle selective (Figure 2B). In addition, only 5.8% were sensitive to grating motion direction (Figure 2C).

To characterize cross-orientation inhibition in grating neurons, we contrasted the peak grating responses and the corresponding plaid responses (blue circles in Figure 2D). The median peak grating response versus plaid response was 0.31 versus 0.14 in monkey A and 0.48 versus 0.27 in monkey B. We also included the plaid neurons' scatterplots from Figure 1F for comparison (yellow circles in Figure 2D). Unlike plaid neurons that were all below the diagonal unity line (plaid facilitation), most grating neurons (95.0% in monkey A and 92.7% in monkey B) were above the unity line, showing cross-orientation inhibition. There was not much overlap between plaid and grating neurons, suggesting two separate neuronal subpopulations.

We also used a cross-inhibition index (CII) to characterize cross-orientation inhibition in each neuron:

$$CII = \frac{R_{plaid} - R_{grating}}{R_{plaid} + R_{grating}}. \quad \text{(Equation 2)}$$

Here, $R_{grating}$ and R_{plaid} represented a neuron's responses to the optimally oriented grating and the corresponding plaid pattern (at the best cross-angle when applicable), respectively. CII < 0 would indicate cross-orientation inhibition. Most grating neurons showed cross-orientation inhibition, with the median CII = −0.36 and −0.39 at 150 μm and 300 μm in monkey A, and −0.31 and −0.29 at 150 μm and 300 μm in monkey B, respectively (Figure 2E).

Busse et al. [11] reported that when the contrast of the orthogonal grating was markedly lower than the optimally oriented grating (e.g., 1 out of 4 of the optimal grating contrast), a neuron's peak response was unchanged by the orthogonal grating, showing no cross-orientation inhibition. We did not observe such effects. When a higher-contrast Gabor (0.32 contrast) at an optimal orientation was superimposed by a lower-contrast orthogonal Gabor (0.08 contrast), the majority of the neurons' peak responses were still suppressed in monkey A. The median CIIs were −0.37 at 150 μm and −0.44 at 300 μm (Figure 2F), similar to the corresponding CIIs at −0.36 and −0.39 in the same neurons with equal component contrasts at 0.32 (Figure 2E).

Co-existence of Plaid Facilitation and Cross-Orientation Inhibition in a Small Portion of Orientation-Tuned Neurons

A small portion of grating neurons (~8%) showed not only cross-orientation inhibition at peak orientations but also plaid facilitation at off-peak orientations. Figure 3A shows the results of 4 exemplar neurons, in which cross-orientation inhibition occurred at peak orientations but plaid facilitation occurred at off-peak orientations.

Overall, the peak grating responses were higher than the plaid responses at off-peak orientations. The median was 0.32 versus 0.23 in monkey A, and 0.44 versus 0.38 in monkey B (Figure 3B). Like previous grating and plaid neurons, those showing both cross-orientation inhibition and plaid facilitation were seldom tuned to grating motion direction (5.5%) and plaid motion direction (2.75%).

V1 neurons are spatially organized on the basis of orientation preferences [12, 13]. Indeed, the orientation maps of grating neurons showed iso-orientation clustering (Figure 4A). To quantify, we calculated the mean correlation coefficient of preferred orientations of cell pairs as a function of absolute cortical distance for each map (Figure 4B). Compared with the baseline pairwise correlations with neurons randomly sampled, the measured pairwise correlations were significantly higher within cortical distances up to 150–200 μm in all maps ($p_s < 0.001$), suggesting that the width of iso-orientation clusters was about 200 μm.

In contrast, the orientation maps of plaid neurons showed no plaid orientation clustering (Figure 4C, calculated with plaids at a 90° cross-angle). There were no significant mean pairwise correlations within a cortical distance of 0–50 μm in each map as compared with the baseline correlations (Figure 4D) ($p_s > 0.07$). (Note that the 3 plaid orientations would have more likely

Figure 1. Plaid Neurons

(A) Visual stimuli: a Gabor grating and three plaid patterns with a cross-angle of 30°, 60°, or 90°.

(B) Responses of exemplar plaid neurons to gratings and plaids. They were insensitive to gratings, but were much more responsive to plaids at a specific plaid orientation. Neurons B60 and B1009 were also cross-angle selective. Error bars are ±1 SEM.

(C) The percentage of plaid neurons that were plaid orientation selective.

(D) The percentage of plaid neurons that were cross-angle selective in monkey B.

(E) The percentage of plaid neurons that were plaid direction tuned.

(F) Peak plaid responses contrasted with higher grating component responses of plaid neurons.

(G) Plaid facilitation index (PFI) distributions of plaid neurons. Red vertical lines indicate medians.

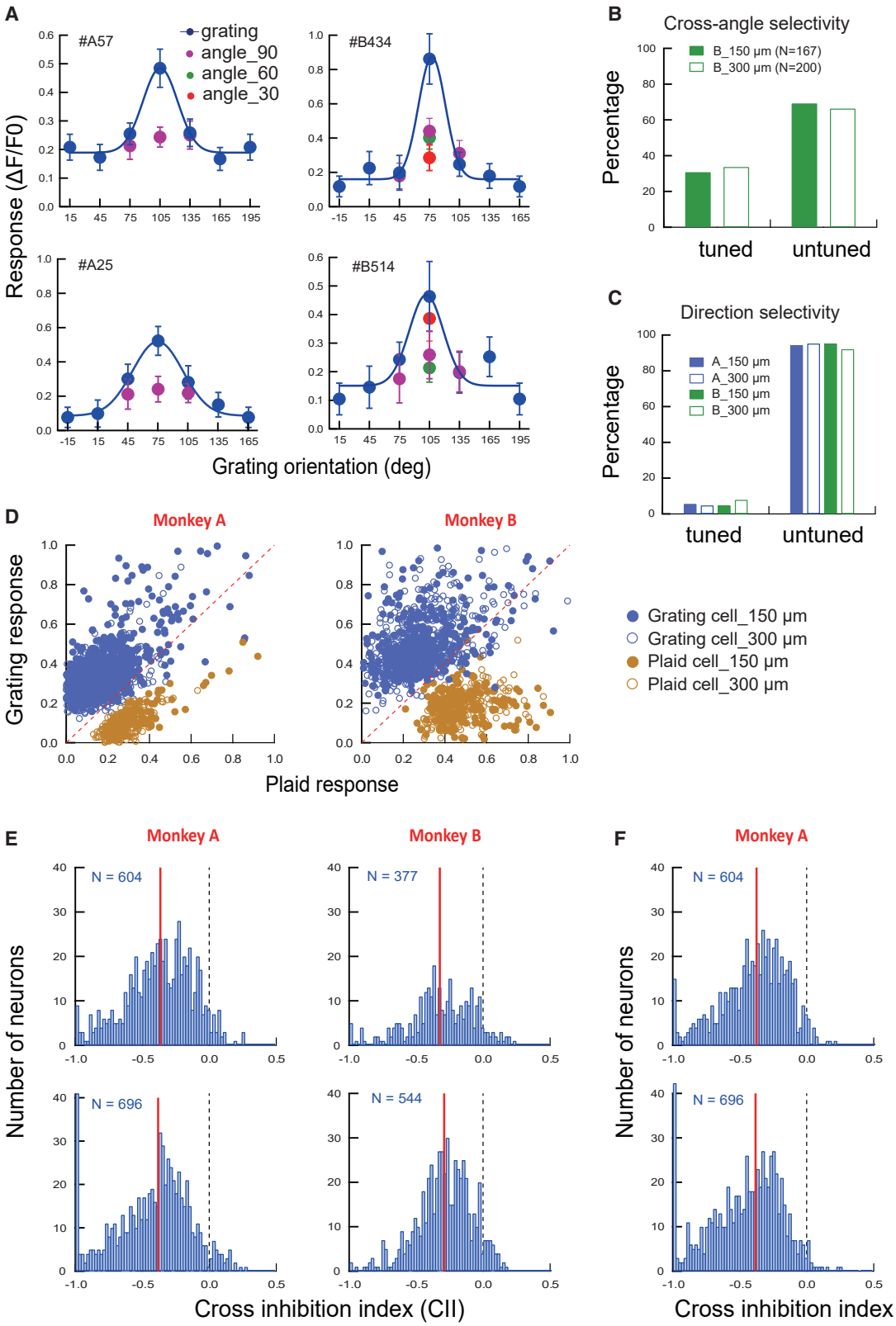

(legend on next page)

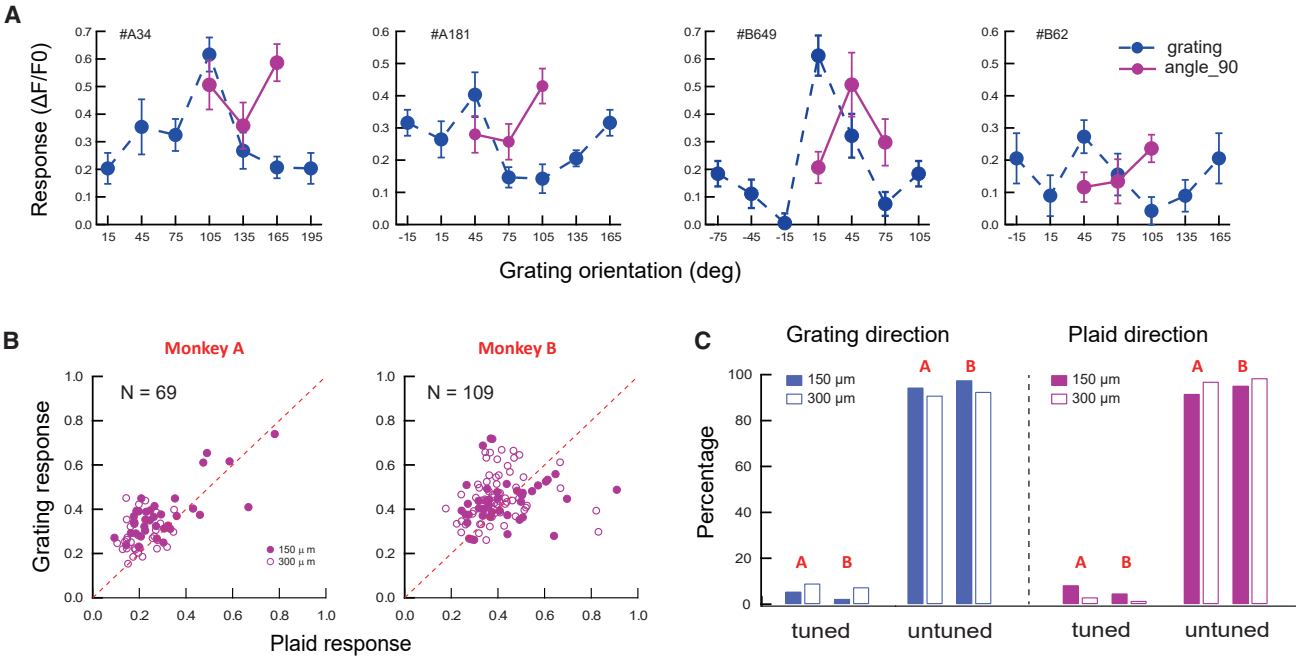

Figure 3. Orientation-Tuned Neurons Showing Both Cross-Orientation Inhibition and Plaid Facilitation

(A) Examples of orientation-tuned neurons that showed both cross-orientation inhibition at peak orientations and plaid facilitation at off-peak grating orientations. Error bars are ±1 SEM.

(B) The peak grating responses and plaid responses at off-peak grating orientations are contrasted.

(C) The percentages of these neurons showing tuning to grating motion direction and plaid motion direction.

revealed plaid orientation clustering, if there were any, than more plaid orientations.)

Psychophysicists have long suspected that the visual cortex contains early mechanisms specialized in processing plaids. For example, adaptation effects to plaids are distinguishable from those to gratings [2, 3]. Moreover, plaid is a pop-out feature in visual search, suggesting that plaid processing is pre-attentive at an early stage of visual processing [1, 4, 5]. Consistent with these psychophysical reports, our study demonstrates plaid neurons in macaque V1 superficial layers that prefer plaids to gratings. Because they are mostly non-orientation tuned, these plaid neurons could be easily missed by conventional single- and multi-unit recordings that typically use oriented stimuli to map the receptive fields of individual neurons.

Plaid neurons have also been reported in mouse V1 superficial layers with two-photon imaging [14, 15]. In these neurons, grating responses are anti-correlated with plaid responses in strength. Only those significantly more responsive to gratings and plaids are classified as grating and plaid neurons, respectively. There are many more neurons that respond to both stimuli similarly. For monkey data, we summarize the results by comparing the peak grating responses to corresponding plaid responses in grating neurons, and the peak plaid responses to corresponding grating component responses in plaid neurons, which shows separated distributions of grating and plaid neurons (Figure 2D). If instead we compare the maximal grating and plaid responses of each neuron, the distributions of grating and plaid neurons become more overlapping (Figure S1). This is because some grating neurons showed higher plaid responses at off-peak grating orientations than at peak grating orientations, and some plaid neurons showed higher grating responses at non-component grating orientations, even if the grating responses were not significantly different across orientations. However, as Figures 2D and S1 indicate, grating responses and plaid responses are positively correlated in both grating and plaid neurons ($r = 0.23$ and 0.56 in Figures 2D and S1, respectively; $p_s < 0.001$), in

Figure 2. Cross-Orientation Inhibition in Orientation-Tuned Neurons

(A) Examples of four individual neurons' grating orientation-tuning functions (blue dots and their Gaussian fittings). At the optimal orientations, the neurons' responses were inhibited by a superimposing grating at a cross-angle of 90° for monkey A (angle_90), and 30°, 60°, and 90° for monkey B (angle_30, angle_60, and angle_90). When the grating rotated ±30° from peak (left and right purple dots), cross-orientation inhibition disappeared. Error bars are ±1 SEM.

(B) The percentage of orientation-tuned neurons that showed cross-angle selectivity of cross-orientation inhibition in monkey B.

(C) The percentage of orientation-tuned neurons that showed direction selectivity.

(D) Peak grating responses contrasted with the corresponding plaid responses (blue dots). Data of plaid neurons from Figure 1F were replotted here for comparison (yellow dots). In addition, comparisons of maximal plaid and grating responses of all grating and plaid neurons are presented in Figure S1.

(E) Distributions of the cross-inhibition index (CII) for orientation-tuned neurons (blue bars). Here CII < 0 indicates cross-orientation inhibition. Red vertical lines indicate medians.

(F) The effect of relative component contrasts on cross-orientation inhibition. CIIs in monkey A were calculated when the peak grating was superimposed by an orthogonal grating at 1/4 of the contrast (0.32 versus 0.08). Red vertical lines indicate medians.

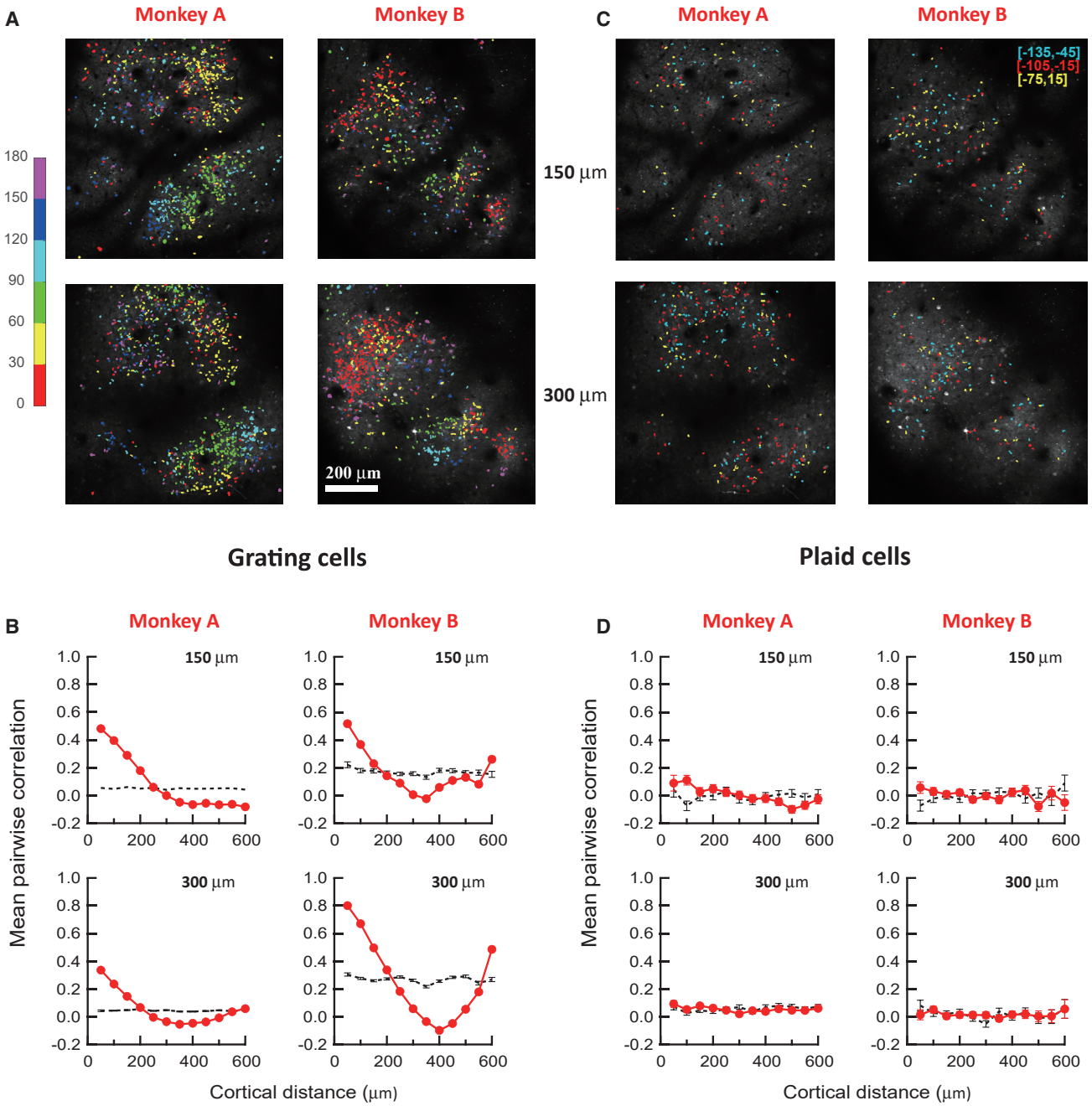

Figure 4. Grating and Plaid Orientation Maps

(A) Grating orientation maps in grating neurons.

(B) The mean correlation of grating orientation tuning of cell pairs as a function of the absolute cortical distance. Each red dot indicates the average measured pairwise correlation within a 50-μm bin up to the dot's corresponding cortical distance on the x axis. The black dashed curves are the baseline pairwise correlations simulated with neurons randomly sampled.

(C) Plaid orientation maps in plaid neurons. The plaid neurons' preferred plaid orientations were defined by two-component orientations shown in brackets.

(D) Mean correlation of plaid orientation tuning of cell pairs as a function of the absolute cortical distance. Error bars are ±1 SEM.

contrast to the negative correlations shown in mouse results. It is thus possible that different processes might be involved in mouse and macaque processing of gratings and plaids.

Nearly all grating neurons have their peak responses more or less suppressed by corresponding plaid patterns. This cross-orientation inhibition effect has often been assumed to contribute to divisive gain control of neural responses [8, 16]. When cross-orientation inhibition and plaid facilitation are considered together, a new picture emerges. That is, grating neurons are excited by gratings and inhibited by plaids, so they are

selectively sensitive to one-dimensional stimuli such as lines and contours, and have minimal interference from two-dimensional plaid-like noises. In parallel, plaid neurons are excited by plaids but are not responsive to gratings, so they are selectively sensitive to two-dimensional stimuli such as line crossings, and have little interference from one-dimensional noises. These push-pull-like effects thus can facilitate precise V1 representations of lines and contours and their crossings in natural scenes.

Including plaid detectors in vision models might simplify the explanation of some texture-related visual processes. One famous example is the Lincoln portrait that becomes difficult to recognize when coarsely quantized. Harmon and Julesz [17] suggested that the difficulty results from high-spatial-frequency noise that masks low-spatial-frequency face information. However, Morrone et al. [18] demonstrated later that adding further high-frequency noise also eases portrait recognition. They suggested that certain neural mechanisms might act to impose block structures on the portrait to impair recognition, which is cancelled by high-frequency noise. It is conceivable that plaid neurons can respond to plaid-like block structures on a quantized image, which disrupts grating neurons' responses to smooth face edges and complicates portrait recognition.

In the motion perception literature, there is evidence that only MT neurons in macaques are responding to the global direction of a moving plaid, and V1 neurons remain tuned to the directions of individual grating components [19]. In our study, only small fractions of plaid neurons (4.3%) and grating neurons (5.8%) are motion direction selective, which is reasonable because layer 2/3 neurons in macaque V1 mainly receive inputs from the P pathway that is insensitive to motion direction. Therefore, these plaid neurons in macaque V1 are more likely plaid pattern detectors, rather than plaid motion detectors.

STAR★METHODS

Detailed methods are provided in the online version of this paper and include the following:

- KEY RESOURCES TABLE
- LEAD CONTACT AND MATERIALS AVAILABILITY
- EXPERIMENTAL MODEL AND SUBJECT DETAILS
  - Rhesus macaques
- METHOD DETAILS
  - Monkey preparation
  - Behavioral task
  - Visual stimuli
  - Two-photon imaging
- QUANTIFICATION AND STATISTICAL ANALYSIS
- DATA AND CODE AVAILABILITY

SUPPLEMENTAL INFORMATION

Supplemental Information can be found online at https://doi.org/10.1016/j.cub.2020.01.005.

ACKNOWLEDGMENTS

This study was supported by Natural Science Foundation of China grants 31230030 and 31730179 and funds from the Peking-Tsinghua Center for Life Sciences, Peking University.

AUTHOR CONTRIBUTIONS

S.-C.G., S.-H.Z., and Y.-C.Z. conducted the experiments, S.-C.G. and C.Y. analyzed data, C.Y. and S.-M.T. designed the experiments, and S.-C.G., C.Y., and S.-M.T. wrote the paper.

DECLARATION OF INTERESTS

The authors declare no competing interests.

Received: September 30, 2019
Revised: November 26, 2019
Accepted: January 2, 2020
Published: February 20, 2020

REFERENCES

1. Nam, J.H., Solomon, J.A., Morgan, M.J., Wright, C.E., and Chubb, C. (2009). Coherent plaids are preattentively more than the sum of their parts. Atten. Percept. Psychophys. *71*, 1469–1477.
2. Peirce, J.W., and Taylor, L.J. (2006). Selective mechanisms for complex visual patterns revealed by adaptation. Neuroscience *141*, 15–18.
3. Robinson, A., and MacLeod, D. (2011). The McCollough effect with plaids and gratings: evidence for a plaid-selective visual mechanism. J. Vis. *11*, 26.
4. Julesz, B. (1981). Textons, the elements of texture perception, and their interactions. Nature *290*, 91–97.
5. Julesz, B., and Bergen, J.R. (1983). Human factors and behavioral science: textons, the fundamental elements in preattentive vision and perception of textures. Bell Syst. Tech. J. *62*, 1619–1645.
6. Li, Z., and Atick, J.J. (1994). Towards a theory of the striate cortex. Neural Comput. *6*, 127–146.
7. Bonds, A.B. (1989). Role of inhibition in the specification of orientation selectivity of cells in the cat striate cortex. Vis. Neurosci. *2*, 41–55.
8. Morrone, M.C., Burr, D.C., and Maffei, L. (1982). Functional implications of cross-orientation inhibition of cortical visual cells. I. Neurophysiological evidence. Proc. R. Soc. Lond. B Biol. Sci. *216*, 335–354.
9. Li, M., Liu, F., Jiang, H., Lee, T.S., and Tang, S. (2017). Long-term two-photon imaging in awake macaque monkey. Neuron *93*, 1049–1057.
10. DeAngelis, G.C., Robson, J.G., Ohzawa, I., and Freeman, R.D. (1992). Organization of suppression in receptive fields of neurons in cat visual cortex. J. Neurophysiol. *68*, 144–163.
11. Busse, L., Wade, A.R., and Carandini, M. (2009). Representation of concurrent stimuli by population activity in visual cortex. Neuron *64*, 931–942.
12. Hubel, D.H., and Wiesel, T.N. (1962). Receptive fields, binocular interaction and functional architecture in the cat's visual cortex. J. Physiol. *160*, 106–154.
13. Bonhoeffer, T., and Grinvald, A. (1991). Iso-orientation domains in cat visual cortex are arranged in pinwheel-like patterns. Nature *353*, 429–431.
14. Ringach, D.L. (2019). The geometry of masking in neural populations. Nat. Commun. *10*, 4879.
15. Tring, E., and Ringach, D.L. (2018). On the subspace invariance of population responses. arXiv, arXiv:1811.03251v1.
16. Heeger, D.J. (1992). Normalization of cell responses in cat striate cortex. Vis. Neurosci. *9*, 181–197.
17. Harmon, L.D., and Julesz, B. (1973). Masking in visual recognition: effects of two-dimensional filtered noise. Science *180*, 1194–1197.
18. Morrone, M.C., Burr, D.C., and Ross, J. (1983). Added noise restores recognizability of coarse quantized images. Nature *305*, 226–228.
19. Movshon, J.A., Adelson, E.H., Gizzi, M.S., and Newsome, W.T. (1985). The analysis of moving visual patterns. In Pattern Recognition Mechanisms, C. Chagas, R. Gattass, and C. Gross, eds. (Vatican Press), pp. 117–151.

STAR★METHODS

KEY RESOURCES TABLE

REAGENT or RESOURCE	SOURCE	IDENTIFIER
Deposited Data		
Data for each figure	This paper	https://github.com/smileyguan2019/macaque2p
Experimental Models: Organisms/Strains		
Rhesus monkeys	Beijing Prima Biotech	http://www.primasbio.com/cn/Default
Recombinant DNA		
AAV1.hSyn.GCaMP5G	Penn Vector Core	V5072MI-R
Software and Algorithms		
MATLAB	MathWorks	MATLAB R2016b
Codes for the movement correction	Peking University	https://github.com/Tangshm/Movement-Correction/projects/1

LEAD CONTACT AND MATERIALS AVAILABILITY

Further information and requests for resources and reagents should be directed to and will be fulfilled by the Lead Contact, Cong Yu (yucong@pku.edu.cn)

This study did not generate new unique reagents.

EXPERIMENTAL MODEL AND SUBJECT DETAILS

Rhesus macaques

Two rhesus macaques (male, 4-5 years old, 5-7 kg) were purchased from Beijing Prima Biotech Inc. and housed at Peking University Laboratory Animal Center. All experimental protocols were approved by the Peking University Animal Care and Use Committee.

METHOD DETAILS

Monkey preparation

Each monkey was prepared with two sequential surgeries under general anesthesia and strictly sterile conditions. In the first surgery, a 20-mm diameter craniotomy was performed on the skull over V1. The dura was opened and 100-150 nL AAV1.hSynap. GCaMP5G.WPRE.SV40 (AV-1-PV2478, titer 2.37e13 (GC/ml), Penn Vector Core) was pressure-injected at a depth of ~350 μm in multiple tracks (17 in Monkey A and 21 in Monkey B, each track covering about 1-mm cortical surface). The dura was then sutured, the skull cap was reattached with three titanium lugs and six screws, and the scalp was sewn up. After the surgery, the animal was returned to the cage, treated with injectable antibiotics (Ceftriaxone sodium, Youcare Pharmaceutical Group, China) for one week. The second surgery was performed 45 days later. A T-shaped steel frame was installed for head stabilization, and an optical window was inserted onto the cortical surface. More details of the preparation and surgical procedures can be found in [9].

Behavioral task

After a ten-day recovery from the second surgery, monkeys were seated in a primate chair with head restraint. They were trained to hold fixation on a small white spot (0.1°) with eye positions monitored by an ISCAN ETL-200 infrared eye-tracking system (ISCAN Inc.) at a 120-Hz sampling rate.

During the experiment, trials with the eye position deviated 1.5° or more from the fixation were discarded as ones with saccades and repeated. For the remaining trials, the eye positions were mostly concentrated around the fixation point. The mean and standard deviation of the eye positions were 0.21°, and 0.18° in Monkey A, and 0.20° and 0.10° in Monkey B. The eye positions were within 0.5° from the fixation point in 92.1% of trials for Monkey A, and in 98.4% of trials for Monkey B.

Detailed analysis indicated that the standard deviations of fixational eye movements were similar along and orthogonal to the grating orientation in each trial (median SD ratio = 1.00 for both monkeys) (Figure S2A). So were the standard deviations of fixational eye movements along two orthogonal component grating orientations of plaids (median SD ratio = 1.08 for Monkey A and 1.00 for Monkey B) (Figure S2A). Therefore, the monkey's fixational eye movements were random and stimulus unspecific. Moreover, linear regression analysis showed that the peak response of each grating neuron was not accounted by the standard deviations of fixational eye movements along and orthogonal to the optimally oriented grating orientation (median R^2 = 0.14 for Monkey A and 0.18 for Monkey B; R^2 was significant ($p < 0.05$) in 7.0% of grating neurons; 12 trials entered the analysis per cell) (Figure S2B). Neither was the

peak response of each plaid neuron by the standard deviations of fixational eye movements along two orthogonal component grating orientations of the optimally oriented plaids (median $R^2 = 0.14$ for Monkey A and 0.11 for Monkey B; R^2 was significant ($p < 0.05$) in 5.4% of plaid neurons; 12 trials entered the analysis per cell) (Figure S2B). These data suggested that the responses of grating neurons and plaid neurons were little affected by fixational eye movements.

Visual stimuli

Visual stimuli were generated by the ViSaGe system (Cambridge Research Systems) and presented on a 21-inch CRT monitor with a refresh rate of 80 Hz. Monitor resolution was set at 1280 pixel × 960 pixel. Because of the space and monitor size limits, viewing distances were 30 cm at lower spatial frequencies (< 2 cpd) and 60 cm at higher spatial frequencies (≥2 cpd). Imaging of all orientations and spatial frequencies at a specific recording depth for one monkey was completed in one session that lasted 3 - 4 hours.

A drifting square-wave grating (3 cycles/s, full contrast, 4 cpd spatial frequency, and 0.4° diameter in size) was first used to determine the population receptive field size and location associated with a recording site (~3° eccentricity), as well as ocular dominance columns when monocularly presented to confirm the V1 location. This process was quick with the use of a 4 × objective lens mounted on the two-photon microscope, which revealed no cell-specific information. After that, cell-specific responses were measured with a drifting Gabor grating (2 cycles/s, 0.9 contrast, 12 equal-spaced orientations, 6 spatial frequencies from 0.25 to 8 cpd in 1-octave steps, 3 sizes for each spatial frequency) to calculate orientation and spatial frequency tuning properties, which were used as references for various experiments. We used this information to decide the optimal spatial frequencies for grating and plaid stimuli for current experiments.

In the experiments, neurons' responses to a single drifting Gabor grating (Figure 1A; 6 equal-spaced orientations, varied from 15° to 165° in 30° steps) at a contrast of 0.32 (Monkey A) or 0.5 (Monkey B) were measured. These Gabor gratings varied in three spatial frequencies (0.71, 1, & 1.41 cpd at 150 μm, and 2.12, 3, & 4.24 cpd at 300 μm) for Monkey A, and two spatial frequencies (2 & 2.83 cpd) for Monkey B. At each spatial frequency the Gabor grating also varied in 3 sizes that were approximately 1, 1.5, and 2 octaves (or σ = 0.42λ, 0.64λ, and 0.85λ) at lower spatial frequencies (< 2 cpd), or 1.5, 2, and 2.5 octaves (or σ = 0.64λ, 0.85λ, and 1.06λ) at higher spatial frequencies (≥2 cpd), respectively (λ for wavelength). The use of three stimulus sizes (always over 1 octave) would help estimate the best response of each neuron with the most center excitation and least surround suppression. The spatial frequency and size that produced the maximal orientation response in a specific cell were selected as the final spatial frequency and stimulus size, upon which the cell's responses to six orientations were used to estimate the orientation tuning function.

Plaid patterns consisting of two drifting Gabor gratings at a cross angle of 90° (Figure 1A) were used for both monkeys and varied at three plaid orientations (formed by component gratings at 15° and 105°, 45° and 135°, and 75° and 165°, respectively). For Monkey B, plaids with cross angles at 30° (component gratings at 45° and 75°, 75° and 105°, and 105° and 135°) and 60° (component gratings at 45° and 105°, 75° and 135°, and 105° and 165°) were also used. The grating components of plaids had the same frequencies, sizes, contrasts as single gratings when grating and plaid responses in a specific cell were compared. For Monkey A, plaids with component contrasts at 0.32 and 0.08, respectively, were also measured to examine the effects of relative component contrasts on cross-orientation inhibition.

The stimuli at a specific viewing distance were pseudo-randomly presented. Each stimulus was presented for 1 s, with an inter-stimulus interval of 1.5 s to minimize the interference of responses from previous trials. Each stimulus condition was repeated 12 times and with half trials for each opposite direction.

Two-photon imaging

Two-photon imaging was performed with a Prairie Ultima IV (*In Vivo*) two-photon microscope (Prairie Technologies) and a Ti:sapphire laser (Mai Tai eHP, Spectra Physics). One recording area of 850 × 850 μm^2 within an 8-mm diameter optical window was selected in each animal and imaged using 1000-nm femtosecond laser under a 16 × objective lens (0.8 N.A., Nikon) at a resolution of 1.6 μm/pixel. Fast resonant scanning mode (32 fps) was chosen to obtain continuous images of neuronal activity (8 fps after averaging every 4 frames). Recordings at two depths for the same monkey were completed in two consecutive days. More details of the two-photon imaging setup can be found in [9].

QUANTIFICATION AND STATISTICAL ANALYSIS

Data were analyzed with customized MATLAB codes. A normalized cross-correlation based translation algorithm was used to reduce motion artifacts [9]. After the correction, fluorescence changes were associated with corresponding visual stimuli through the time sequence information recorded by Neural Signal Processor (Cerebus system, Blackrock Microsystem). By subtracting the mean of the 4 frames before stimuli onset (*F0*) from the average of the 6th-9th frames after stimuli onset (*F*) across 6 repeated trials for the same stimulus condition (same orientation, spatial frequency, size, and drifting direction), the differential images ($\Delta F = F - F0$) were obtained. These differential images were then filtered with a band-pass Gaussian filter (size = 10-20 pixels). Finally, connected subsets of pixels (> 25 pixels) with average pixel value > 3 standard deviations of the mean brightness were classified as regions of interests (ROIs) or potential neurons.

Once the ROIs or potential neurons were decided, the ratio of fluorescence change ($\Delta F/F0$) was calculated as neuronal responses. Each stimulus condition was presented for 12 trials, half for each of two opposite directions. For a specific neuron's response to a specific stimulus condition, the $F0_n$ of the n-th trial was the average of 4 frames before stimulus onset, and F_n was the average

of 5th-8th or 6th-9th frames after stimulus onset, whichever was greater. $F0_n$ was then averaged across 12 trials to obtain the baseline F0 for all trials (for the purpose of reducing variations), and $\Delta F_n/F0 = (F_n\text{-}F0)/F0$ was taken as the neuron's response to this stimulus at this trial.

Several steps were taken to decide whether a neuron was an orientation selective neuron. (1) The optimal spatial frequency, size, and orientation for producing the maximal response were selected for each neuron. Then responses to 6 orientations were decided at the optimal spatial frequency and size. (2) To select orientation-tuned neurons, a non-parametric Friedman test was performed to test whether a neuron's responses at 6 orientations were significantly different from each other. To reduce Type-I errors, we set the significance level at $\alpha = 0.01$. The remaining ones were taken as non-orientation-tuned neurons.

Next, several steps were used for selecting plaid neurons from non-orientation-tuned neurons. (1) The optimal spatial frequency, size, plaid orientation, and cross angle (Monkey B only) for producing the maximal response were selected for each neuron. Then the responses to 3 plaid orientations and 6 grating orientations were decided at the optimal spatial frequency and size. (2) A Wilcoxon signed rank test examined whether the response to an optimal plaid was significantly higher than the higher response to one of two corresponding component gratings ($\alpha = 0.05$). Those showing higher plaid responses were classified as plaid neurons.

To decide whether a plaid neuron was tuned to plaid orientation, its responses to three plaid orientations (at the optimal cross angle in Monkey B) were compared with a non-parametric Friedman test ($\alpha = 0.05$). To decide whether a plaid neuron was tuned to cross angle (only measured in Monkey B), its responses to the three cross angles, regardless of the plaid orientation, were compared with a Friedman test ($\alpha = 0.05$).

Pairwise correlation: Within each orientation map, every neuron pair's correlation coefficient of responses to 6 grating orientations or 3 plaid orientations was calculated. The correlations of all neuron pairs within a specific range of cortical distance (from 0-600 μm in 50 μm steps) were then averaged as the mean pairwise correlation of this range of cortical distance to index orientation clustering.

DATA AND CODE AVAILABILITY

Data and MATLAB code in this study can be found at https://github.com/smileyguan2019/macaque2p.